# Supporting Information

## Conformal Phase-Transition Hydrogel Interfaces for High Fidelity Electrophysiological Sensing and Data-Driven Inference

*Xuelin Li[a], Weiyang Tang[b], Mingyang Wang[a], Giacomo Moretti[c], Ji Lin[a*], Chuanqian Shi[a,d,e*]*

a. Center for Mechanics Plus under Extreme Environments, School of Mechanical Engineering and Mechanics, Ningbo University, Ningbo 315211, China

b. Faculty of Georesources and Materials Engineering, RWTH Aachen University, Aachen 52062, Germany

c. Department of Industrial Engineering, University of Trento, Trento, 38123, Italy

d. Key Laboratory of Impact and Safety Engineering, Ministry of Education, Ningbo University, Ningbo 315211, Zhejiang, China

e. Shaoxing Yuanju Technology Co., Ltd, Shaoxing 311816, Zhejiang, China

*Corresponding author. Email: shichuanqian@nbu.edu.cn; linji@nbu.edu.cn

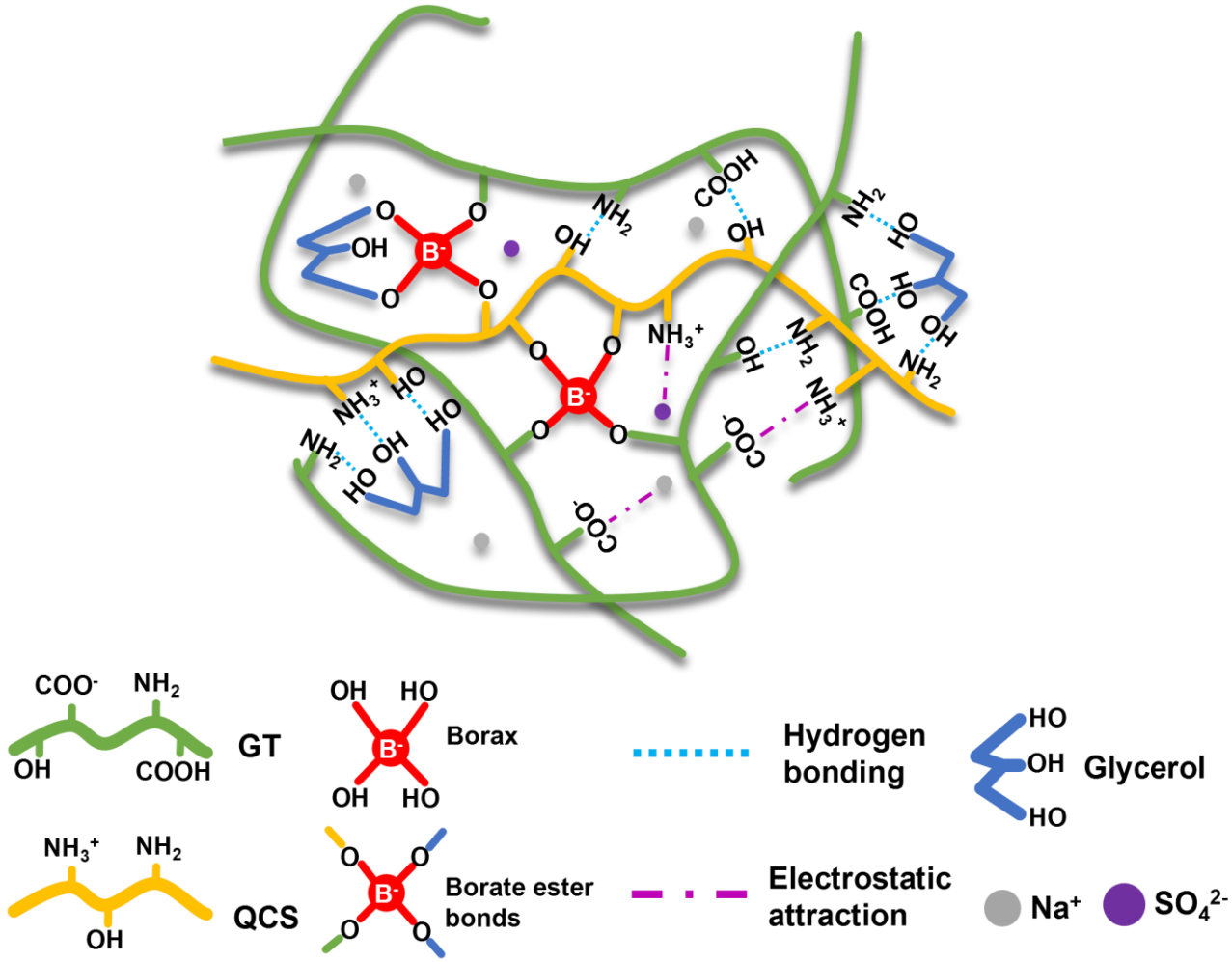


**Figure S1.**

**Composition and structure of the GT-QCS hydrogel.** Schematic illustration of the interpenetrating network within the hydrogel, showing the key components: gelatin (GT), quaternary ammonium chitosan (QCS), borax, $Na_2SO_4$, and the glycerol-water solvent system. Key molecular interactions (ionic interactions, hydrogen bonds, borate-mediated dynamic crosslinks) are highlighted.

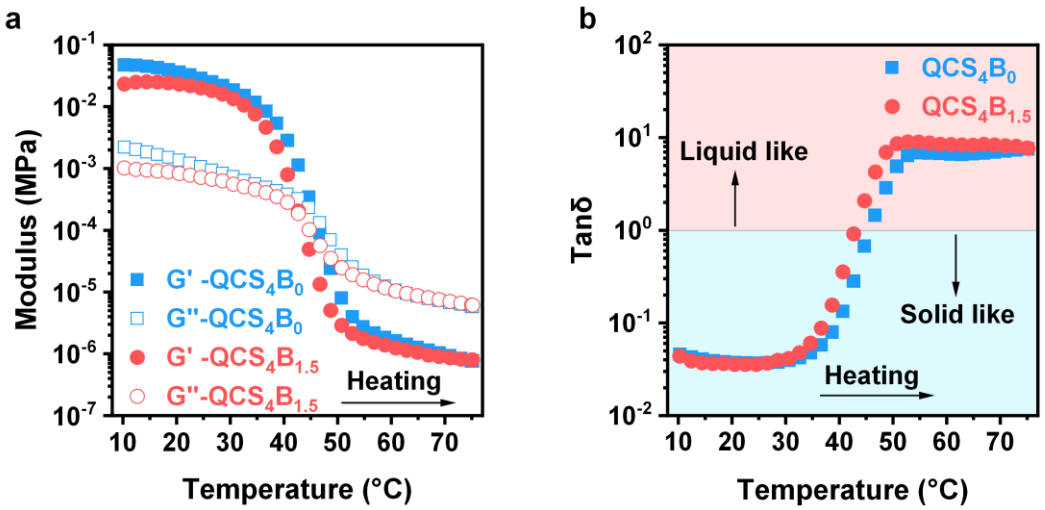


**Figure S2.**

**Rheological test. a)** Rheological characterization of hydrogel solutions with different recipes at a temperature sweep from 10℃ to 75℃, showing their transition between viscoelastic gel state and viscous liquid state. **b)** The corresponding tanδ (G″/G′) calculated from (**a**).

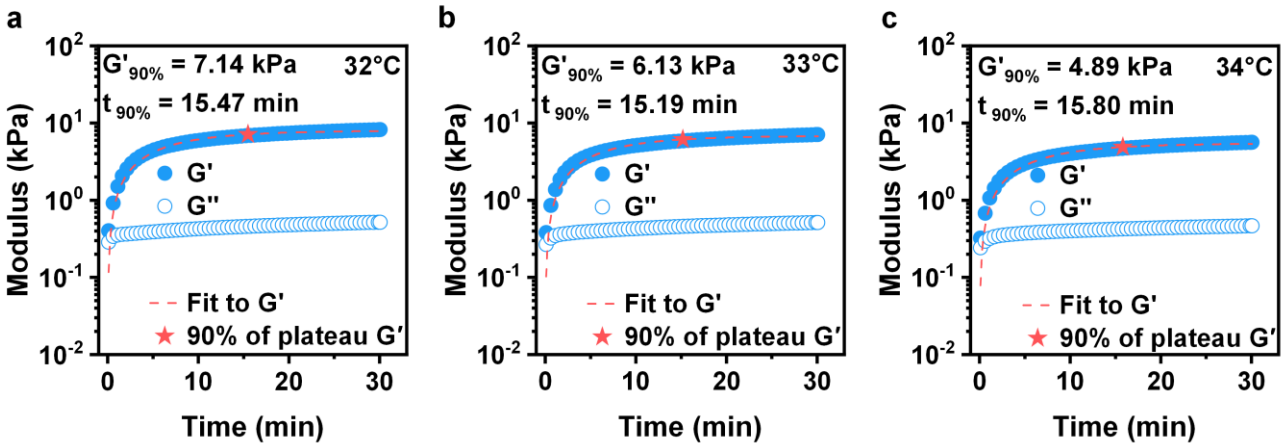


**Figure S3.**

**Isothermal time-sweep rheological characterization of the GT-QCS hydrogel at skin-relevant temperatures. (a-c)** Time-dependent evolution of storage modulus (G′) and loss modulus (G″) at 32°C, 33°C, and 34°C, respectively, over 30 min. Dashed lines represent exponential fitting of G′ using the following equation

$$G'(t) = G'_{max} \times (1 - e^{-kt}) \quad \text{(S1)}$$

where $G'(t)$ is the storage modulus at time $t$, $G'_{max}$ is the equilibrium storage modulus, $k$ is the gelation rate constant, and $t$ is the time. Stars indicate the time point at which G′ reaches 90% of the plateau value.

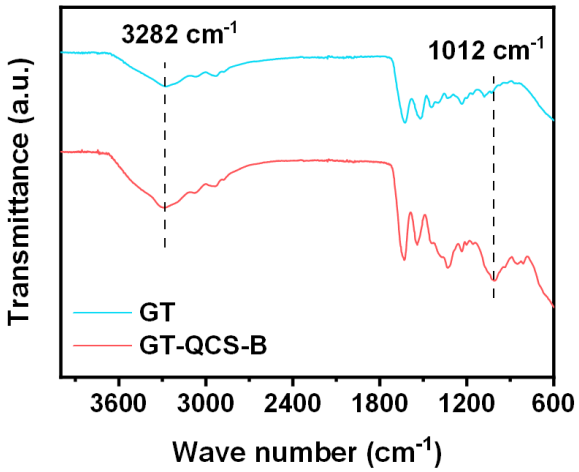


**Figure S4.**

**FTIR spectra of pristine gelatin (GT) and the borax-containing GT-QCS hydrogel (GT-QCS-B).** Compared with GT, GT-QCS-B shows an altered broad O-H stretching band around 3282 $cm^{-1}$ and a distinct spectral change near 1012 $cm^{-1}$. The 1400-1000 $cm^{-1}$ region has been reported to contain characteristic absorptions associated with polymer-borate ester bonds (B-O-C),[58] although overlapping contributions from C-O and C-O-C vibrations may also be present. These spectral changes therefore provide supporting evidence for borate-mediated crosslinking in the GT-QCS-B network.

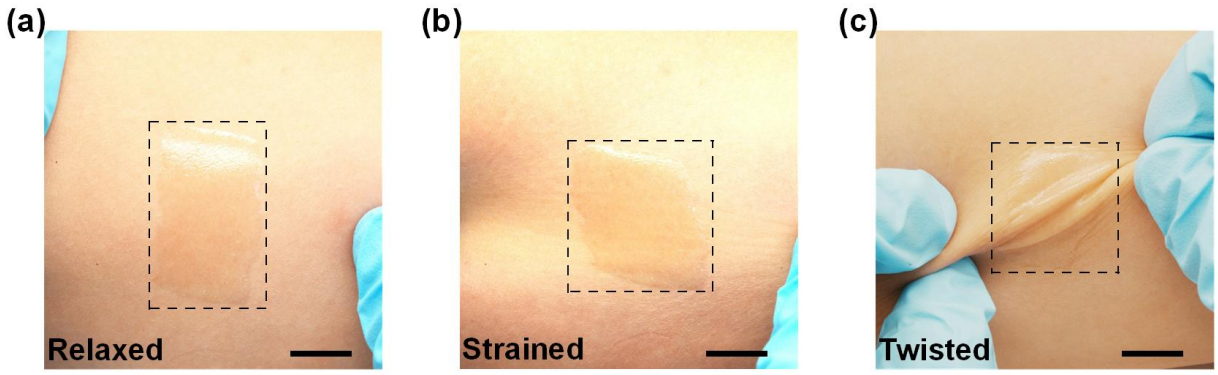


**Figure S5.**

**Skin compliance of the GT-QCS hydrogel. a)** The GT-QCS adhered to human skin in a relaxed state. It conforms to natural skin movements during **b)** compression and **c)** stretching. Scale bar, 10 mm

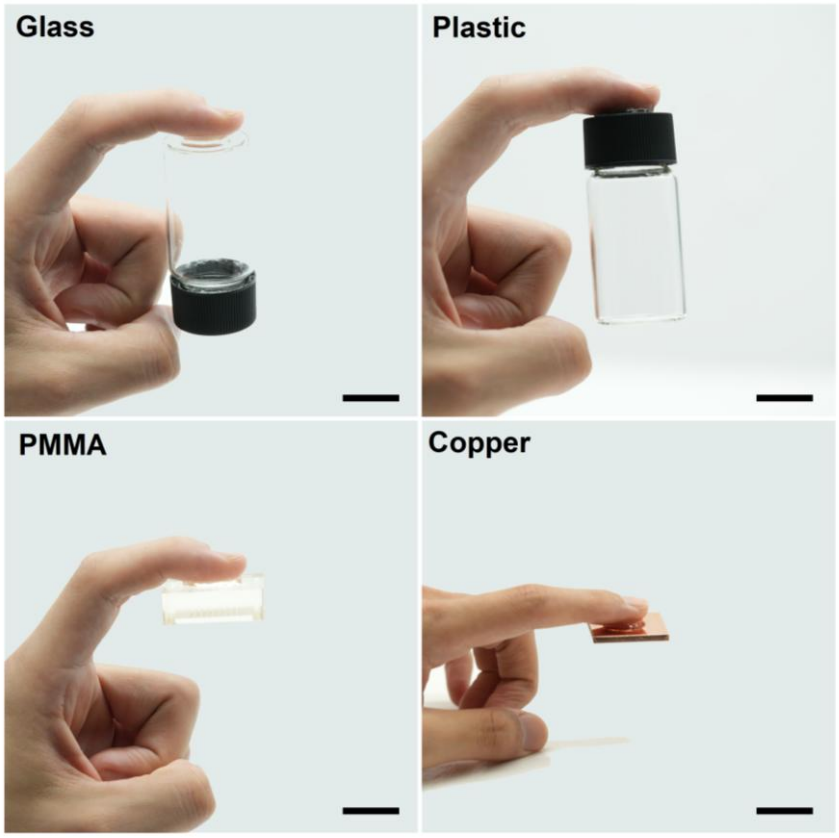


**Figure S6.**

**Adhesion performance of the GT-QCS on various substrates.** Photographs demonstrating the strong adhesion of the GT-QCS hydrogel, enabling it to suspend various objects from a finger: glass, plastic, poly(methyl methacrylate) (PMMA), and copper. Scale bar, 10 mm.

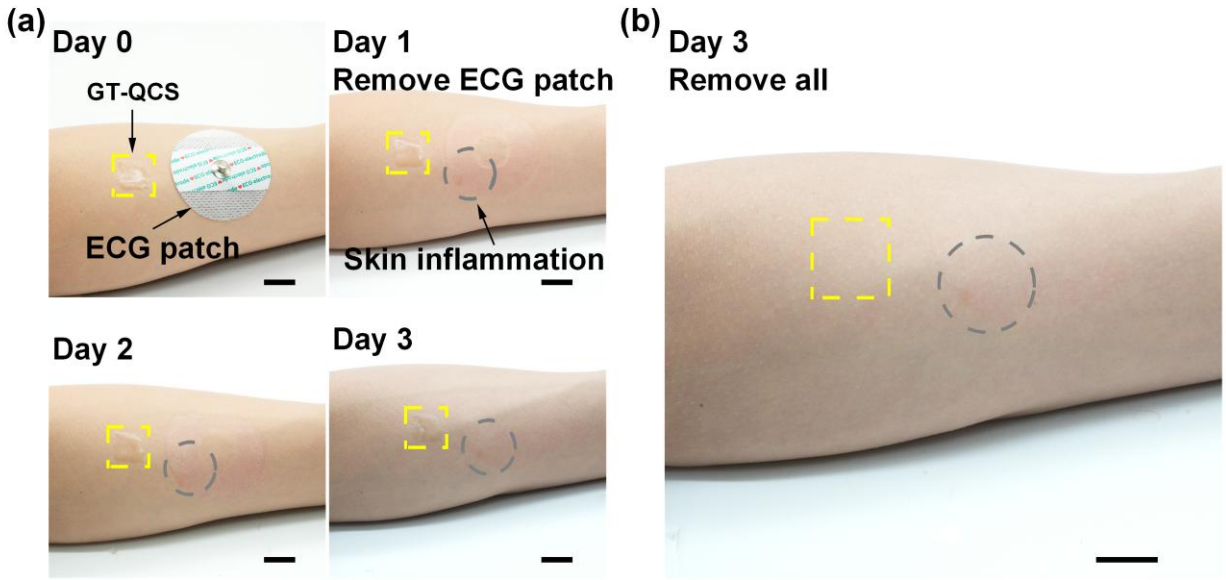


**Figure S7.**

**Assessment of skin compatibility of the GT-QCS over 3 days. a)** Photographs of the GT-QCS electrode and a commercial ECG patch applied simultaneously to the forearm; the commercial ECG patch was removed after 1 day, whereas the GT-QCS electrode remained in place for 3 days. Scale bar, 10 mm. **b)** Corresponding photographs of the skin sites immediately after electrode removal on day 3. Scale bar, 10 mm.

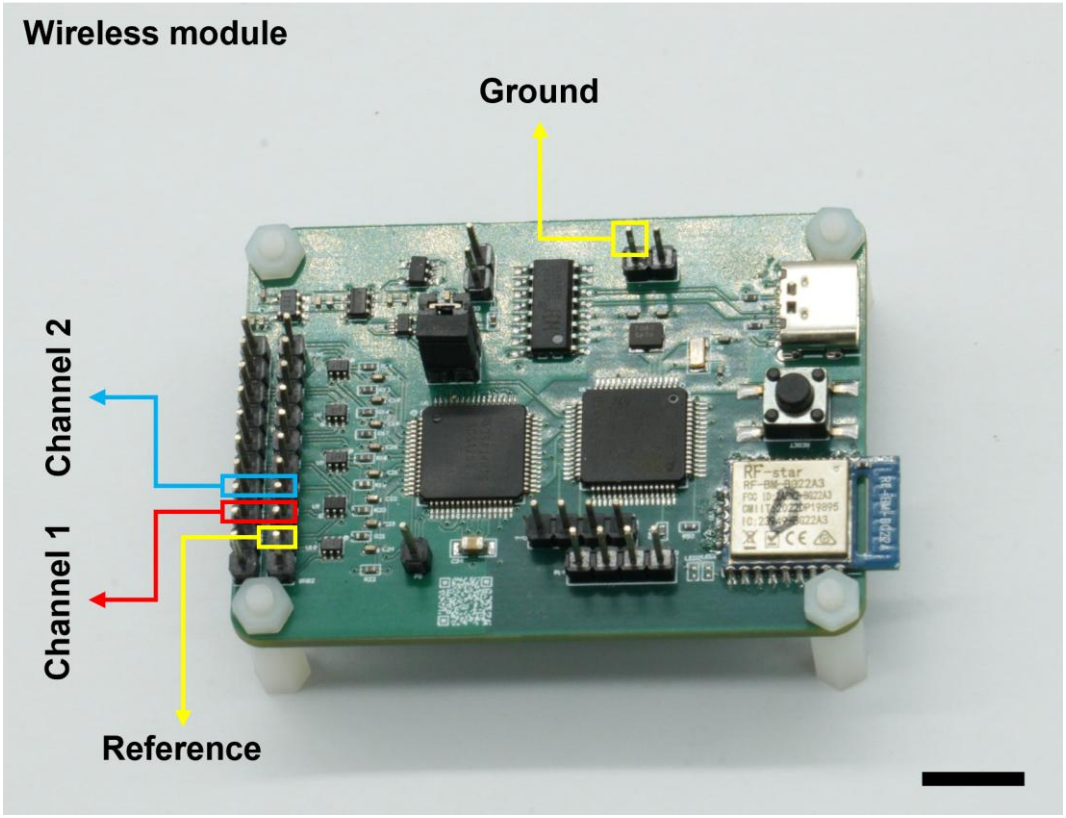


**Figure S8.**

**Photograph of the measurement setup for ECG and EEG wireless monitoring.** A photograph of the ECG and EEG wireless data acquisition module (Zouxian Trading Co., Ltd., Guangzhou, China) with a sampling rate of 250 Hz. Scale bar, 10 mm.

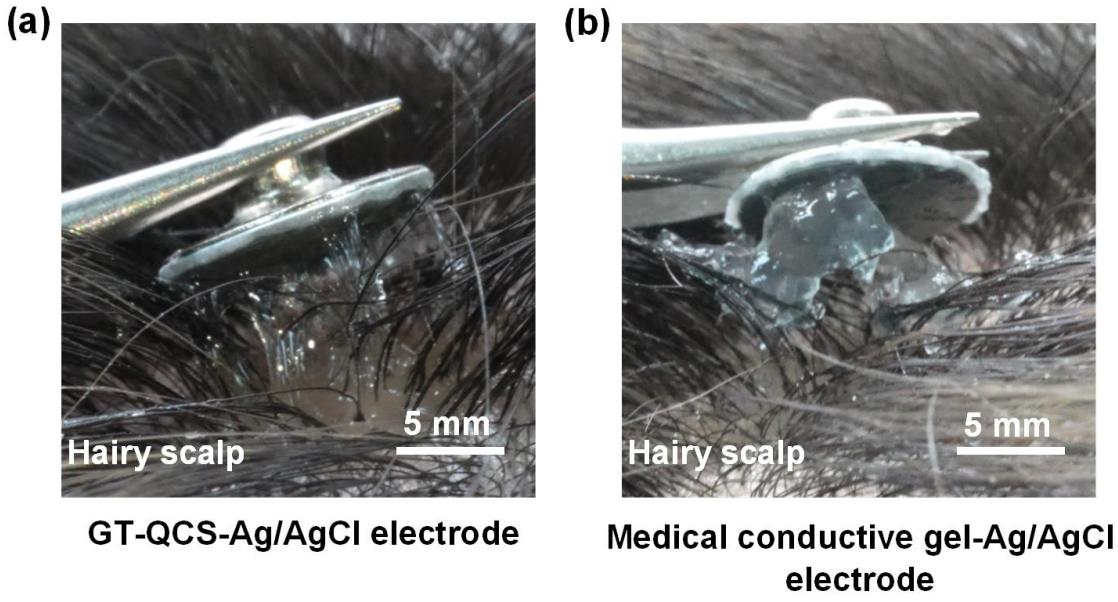


**Figure S9.**

**Comparison of electrode removal behavior on the hairy scalp.** Photographs showing the state of the Ag/AgCl electrodes during removal from the hairy scalp after application with **a)** GT-QCS and **b)** medical conductive gel.

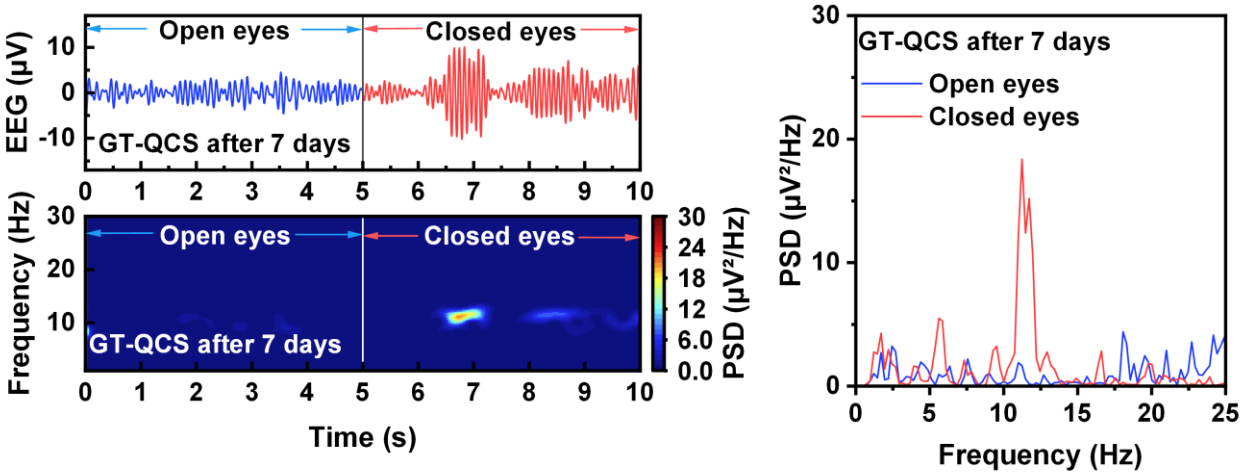


**Figure S10.**

**EEG monitoring performance of the hydrogel electrode after 7 days. a)** Filtered (8–13 Hz) EEG signals captured by the GT-QCS hydrogel electrode during a 5 s eyes-open (EO) / 5 s eyes-closed (EC) protocol. **b)** PSD during EO and EC periods for the GT-QCS electrode, showing the clear emergence of the α-band (8-13 Hz) peak during EC. **c)** Time-frequency analysis plots for the GT-QCS hydrogel electrode, demonstrating suppression of α-band activity during EO and its immediate resurgence upon EC.

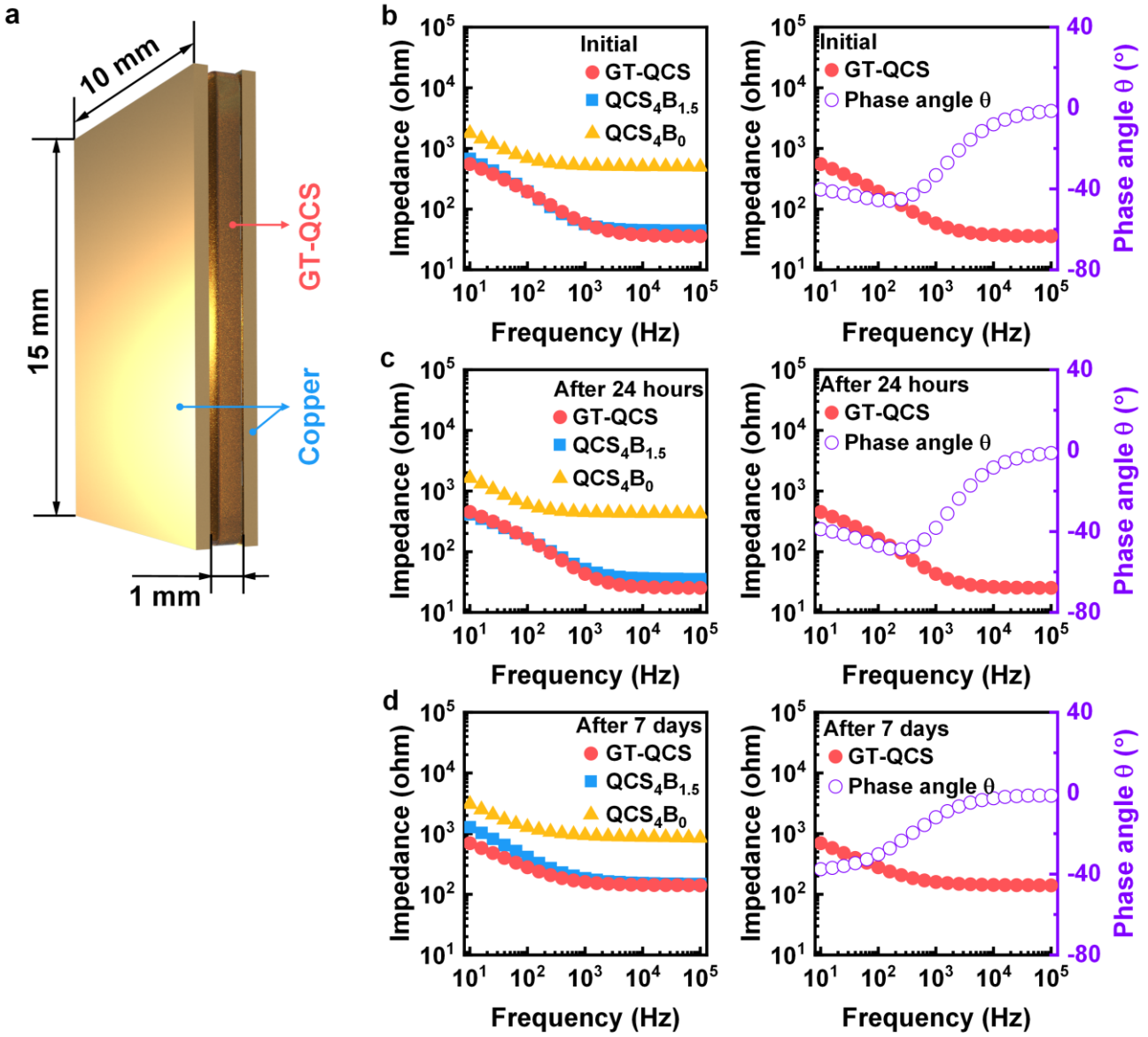


**Figure S11.**

**Intrinsic impedance characterization of GT-QCS hydrogel. a)** Schematic of the experimental setup for measuring the intrinsic impedance of hydrogel samples sandwiched between copper plates. (**b-d)** Intrinsic impedance of hydrogels with different formulations across a frequency range of 10 Hz to 100 kHz, measured on Day 0, Day 1, and Day 7. In each panel, the left plot shows impedance magnitude for all formulations, while the right plot shows impedance magnitude and phase angle (θ) for the GT-QCS formulation.

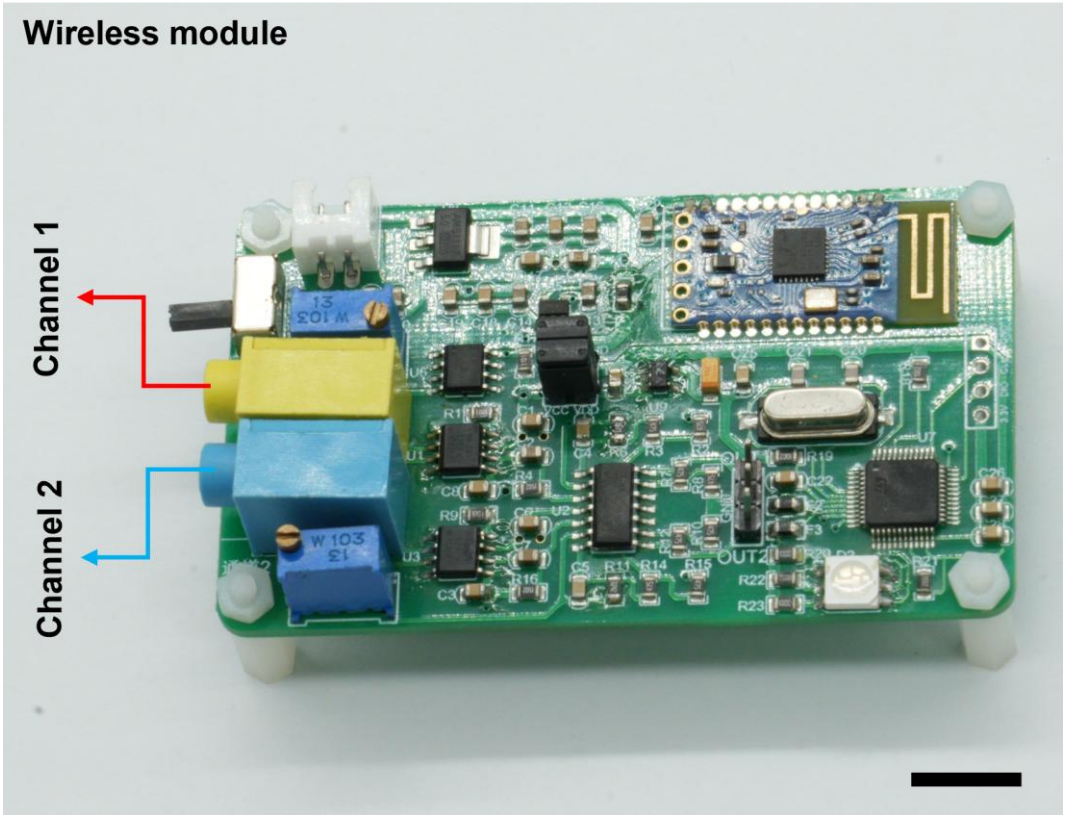


**Figure S12.**

**Photograph of the measurement setup for sEMG wireless monitoring.** A photograph of the wireless data acquisition module (Sichiray Technology Co., Ltd., Wuxi, China) with a sampling rate of 1000 Hz. Scale bar, 10 mm.

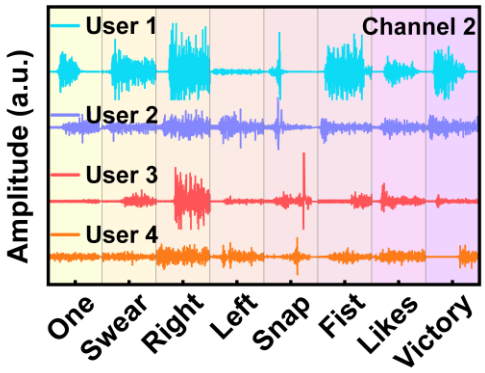


**Figure S13.**

**Comparison of channel 2 sEMG waveforms for eight hand gestures across four subjects.** Representative raw channel-2 sEMG signals from four volunteers performing eight predefined hand gestures. Complementing the channel-1 comparisons shown in Fig. 5c in the main text.

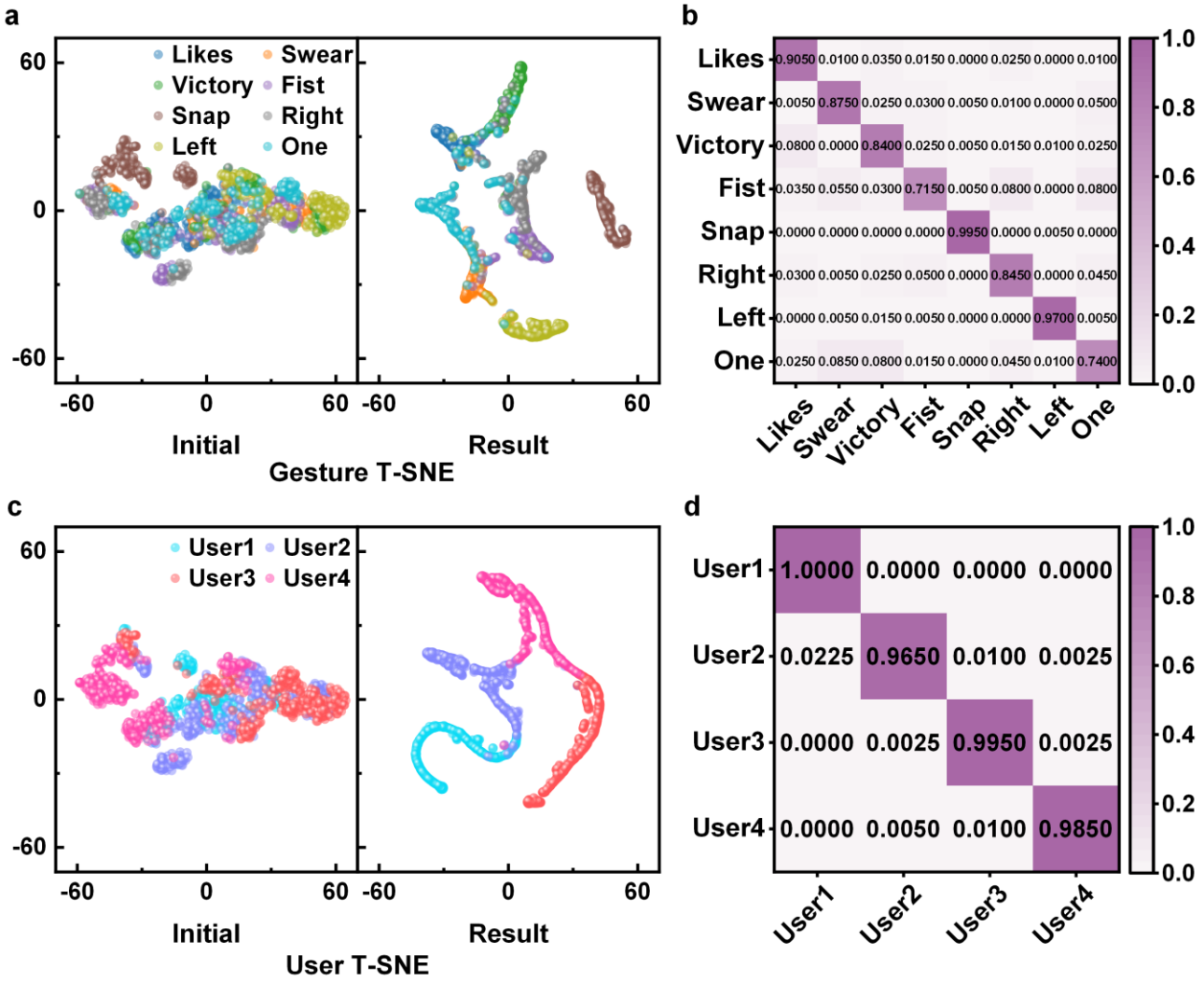


**Figure S14.**

**Results of single-channel sEMG (channel 1) model for gesture and subject classification. a)** Two-dimensional t-SNE visualizations of features for the gesture classification task before (left) and after (right) training. **b)** Confusion matrix for the gesture classification task. **c)** Two-dimensional t-SNE visualizations of features for the subject identification task before (left) and after (right) training. **d)** Confusion matrix for the subject identification task.

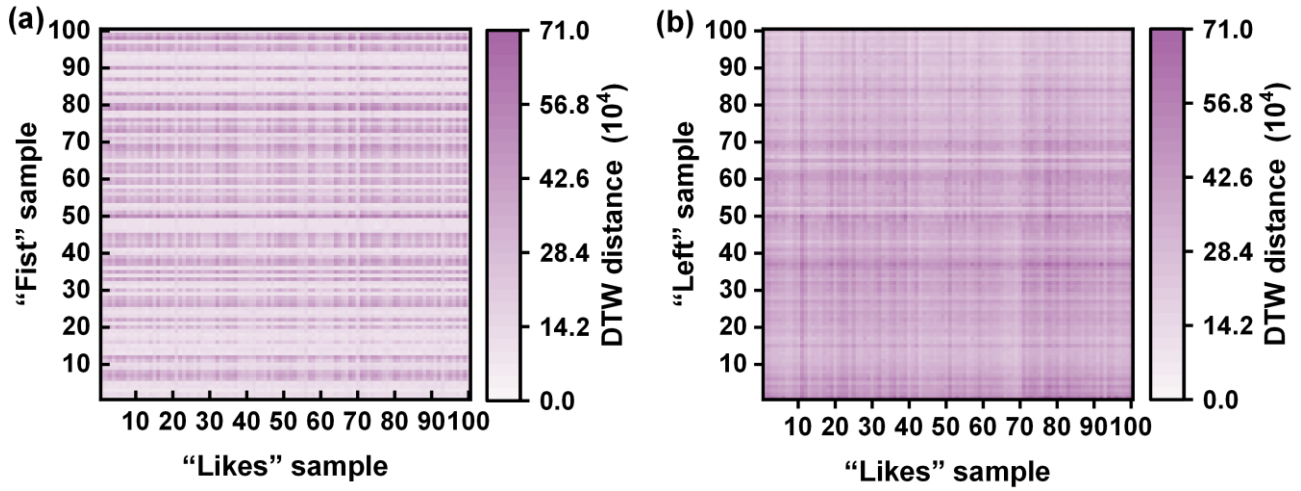


**Figure S15.**

**Dynamic time warping (DTW) analysis of inter-gesture sEMG waveform similarity.-a)** DTW heatmap between the "Fist" and "Likes" gestures. Larger regions of lighter shading indicate lower DTW distance and higher temporal similarity, explaining the model's confusion between these two gestures. **b)** DTW heatmap between the "Left" and "Likes" gestures. More extensive darker regions reflect higher DTW distance and lower temporal similarity, indicating distinct waveform patterns that are easier for the model to discriminate. Heatmap intensity corresponds to the local DTW distance between aligned time-series segments (n = 100 samples per gesture).

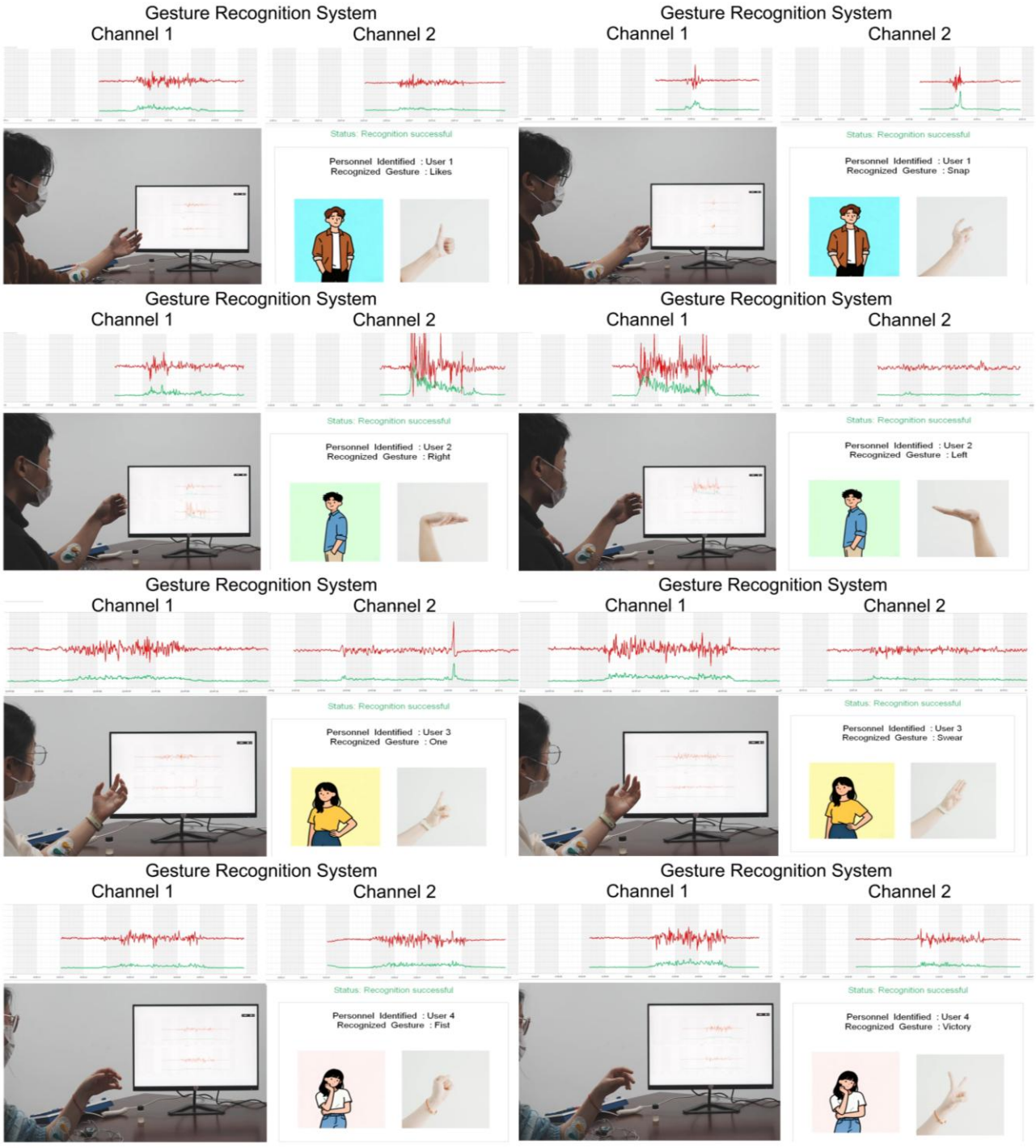


**Figure S16.**

**Representative results of simultaneous gesture and subject identity recognition based on dual-channel sEMG predictions.** From left to right, they are User1-Likes, User1-Snap, User2-Right, User2-Left, User3-One, User3-Swear, User4-Fist, and User4-Victory.

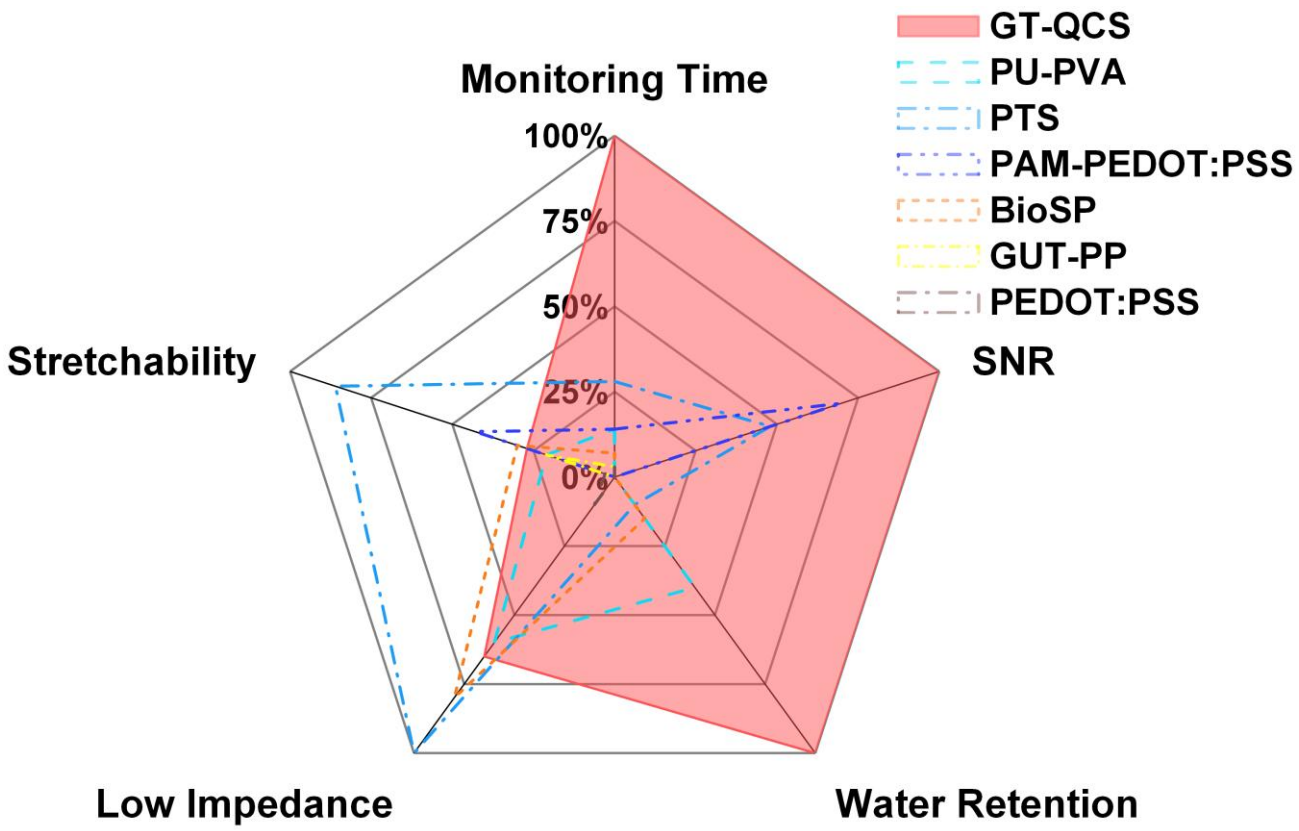


**Figure S17.**

Radar plot comparing normalized performance metrics of the GT-QCS hydrogel electrode with recent literature. Scores (0–100) were derived via min-max normalization from Table S1 (impedance inversely scaled; signal-to-noise ratio (SNR) restricted to ECG values). GT-QCS exhibits a balanced profile with top scores in monitoring duration, SNR, and water retention, competitive impedance, and moderate stretchability.

**Table S1. Comparison of key performance metrics between the GT-QCS hydrogel electrode and recently reported advanced hydrogel electrodes.**

| Materials | Monitoring Duration | SNR | Water Retention | Skin-Contact Impedance | Adhesion Strength | Stretchability | Ref. |
|---|---|---|---|---|---|---|---|
| PU-PVA Tattoo Electrode | >24 h | -- | >81.4% (7 days) | 21.0 kΩ | 2060 μJ·cm$^{-2}$ | 313% | 76 |
| PTS Antibacterial Gel | 48 h | EMG 22.2 dB | Anti-drying described | 4.1 kΩ | 2.8 kPa (shear) | 1300% | 77 |
| PAM-PEDOT:PSS | 24 h | ECG 32.7 dB | -- | -- | Moderate | 646% | 78 |
| BioSP Dual-Network Gel | >12 h | Higher than commercial | 48 h (PDMS) | ~10 kΩ | 40 kPa (shear) | ~450% | 79 |
| GUT-PP Multimodal Gel | Hours | -- | -- | Lower than pure PEDOT | 10.1 kPa (porcine skin) | 322% | 80 |
| PEDOT:PSS Hybrid Film | Short-term | ECG noise 11.8 μV | -- | 256 kΩ·cm$^2$ (10 Hz) | 320 mN·cm$^{-1}$ | 54% | 81 |
| GT-QCS (This work) | 7 days | ECG; EEG; sEMG: ~44.0 dB;~9 dB; ~46.3 dB | ~87.1% (30 days) | 17.96 kΩ | 544.1 mN·cm$^{-1}$ (90° peel) | ~400% | This work |

**Table S2. Summary of experimental parameters, acquisition settings, environmental conditions, and control specifications used in this study.**

| Category | Experiment | Electrode / sample dimensions | Key settings | Environmental conditions | Control / comparison |
|---|---|---|---|---|---|
| Rheology | Temperature sweep | ~1 mL | 2°C·min$^{-1}$ | Room temperature | Different formulations |
| | Isothermal time sweep | | 32°C, 33°C and 34°C | | |
| Mechanical characterization | Tensile | 12 × 2 × 1 mm | 10 mm min$^{-1}$ | 25°C after 30 min curing | Different formulations |
| | Compression | 9 × 9 mm | | | |
| Adhesion | 90° peel test (porcine skin) | 20 × 10 mm (Bonding area) | 10 mm min$^{-1}$ | Cured for 5 min | Medical conductive gel |
| Moisture management | WVTR | 20 × 0.6 mm | Mass-loss method | 25°C; 30% RH | Open vial, Ecoflex |
| | Anti-drying | thickness 1 mm | | | Glycerol-free control |
| Electrical characterization | Intrinsic impedance | 15 × 10 × 1 mm | 10 Hz-100 kHz | Day 0, 1 and 7 | Different formulations |
| | skin-electrode contact impedance | 10 × 1 mm | 10 Hz-10 kHz | Day 0 and 7 | Commercial ECG electrode |
| sEMG recording | Forearm gesture recognition | Diameter 10 mm | Sampling rate: 1000 Hz | Skin cleaned with 75% alcohol | 4 healthy volunteers (forearm) |
| | lumbar movement recognition | | | | 1 healthy volunteer (lumbar) |
| ECG recording | Multi-scenario ECG monitoring | Diameter 10 mm | Sampling rate: 250 Hz | Rest, post-exercise, sleep and work | Commercial ECG electrode |
| EEG recording | Occipital EEG monitoring | Diameter 10 mm | O2 position; sampling rate: 250 Hz | EO and EC paradigm | Medical conductive gel |

**Table S3. Fitting parameters obtained from isothermal time-sweep rheology of the GT-QCS hydrogel at skin-relevant temperatures.**

| Temperature (°C) | $G'_{90\%}$ (kPa) | $G'_{max}$ (kPa) | $k$ (min$^{-1}$) | $t_{90\%}$(min) | $R^2$ |
|---|---|---|---|---|---|
| 32 | 7.14 | 7.93 | 0.1489 | 15.47 | 0.984 |
| 33 | 6.13 | 6.81 | 0.1516 | 15.19 | 0.980 |
| 34 | 4.89 | 5.43 | 0.1457 | 15.80 | 0.982 |

**Table S4. Signal-to-noise ratio (SNR) of EEG signals acquired by the GT-QCS hydrogel electrode and a commercial medical conductive paste on Day 1 and after seven days of continuous wear.**

| Day | Electrode type | Time-domain SNR (dB) | Frequency-domain SNR (dB) |
|---|---|---|---|
| Day 1 | GT-QCS | 9.02 | 18.59 |
| | Medical conductive gel | 10.54 | 14.91 |
| Day 7 | GT-QCS | 8.99 | 15.80 |
| | Medical conductive gel | The medical conductive gel was fully dehydrated by day 7 and therefore no reliable EEG signal could be obtained | |

**Table S5. Detailed classification report for the six-class lumbar movement recognition task based on the dual channel model.**

| Movement Class | Precision | Recall | F1-Score | Support (Samples) |
|---|---|---|---|---|
| Squat | 1.000 | 1.000 | 1.000 | 50 |
| Body flexion | 0.980 | 0.980 | 0.980 | 50 |
| Right-body flexion | 1.000 | 1.000 | 1.000 | 50 |
| Left-body flexion | 0.980 | 0.980 | 0.980 | 50 |
| Left-pistol squat | 1.000 | 1.000 | 1.000 | 50 |
| Right-pistol squat | 1.000 | 1.000 | 1.000 | 50 |
| **Macro Avg** | **0.993** | **0.993** | **0.993** | **300** |
| **Overall Accuracy** | **--** | **--** | **0.993** | **300** |

**Table S6. Detailed classification report for the eight-class hand gesture recognition task based on the dual channel CNN-GRU model.**

| Gesture Class | Precision | Recall | F1-Score | Support (Samples) |
|---|---|---|---|---|
| Likes | 0.869 | 0.965 | 0.915 | 200 |
| Swear | 0.932 | 0.960 | 0.946 | 200 |
| Victory | 0.947 | 0.900 | 0.923 | 200 |
| Fist | 0.927 | 0.890 | 0.908 | 200 |
| Snap | 0.990 | 1.000 | 0.995 | 200 |
| Right | 0.990 | 0.965 | 0.977 | 200 |
| Left | 0.985 | 0.990 | 0.988 | 200 |
| One | 0.932 | 0.895 | 0.913 | 200 |
| **Macro Avg** | **0.947** | **0.946** | **0.946** | **1600** |
| **Overall Accuracy** | **--** | **--** | **0.946** | **1600** |

**Table S7. Detailed classification report for the four-class subject identification task based on the dual channel CNN-GRU model.**

| Gesture Class | Precision | Recall | F1-Score | Support (Samples) |
|---|---|---|---|---|
| User 1 | 0.995 | 1.000 | 0.998 | 400 |
| User 2 | 0.995 | 0.995 | 0.995 | 400 |
| User 3 | 0.990 | 1.000 | 0.995 | 400 |
| User 4 | 1.000 | 0.985 | 0.992 | 400 |
| **Macro Avg** | **0.995** | **0.995** | **0.995** | **1600** |
| **Overall Accuracy** | **--** | **--** | **0.995** | **1600** |

**Table S8. Detailed classification report for the hand gesture recognition task using the single channel ablation model.**

| Gesture Class | Precision | Recall | F1-Score | Support (Samples) |
|---|---|---|---|---|
| Likes | 0.838 | 0.905 | 0.870 | 200 |
| Swear | 0.845 | 0.875 | 0.860 | 200 |
| Victory | 0.800 | 0.840 | 0.820 | 200 |
| Fist | 0.836 | 0.715 | 0.771 | 200 |
| Snap | 0.985 | 0.995 | 0.990 | 200 |
| Right | 0.828 | 0.845 | 0.837 | 200 |
| Left | 0.975 | 0.970 | 0.972 | 200 |
| One | 0.775 | 0.740 | 0.757 | 200 |
| **Macro Avg** | **0.860** | **0.861** | **0.860** | **1600** |
| **Overall Accuracy** | **--** | **--** | **0.861** | **1600** |

**Table S9. Detailed classification report for the subject identification task using the single-channel ablation model.**

| Gesture Class | Precision | Recall | F1-Score | Support (Samples) |
|---|---|---|---|---|
| User 1 | 0.978 | 1.000 | 0.989 | 400 |
| User 2 | 0.992 | 0.965 | 0.978 | 400 |
| User 3 | 0.980 | 0.995 | 0.988 | 400 |
| User 4 | 0.995 | 0.985 | 0.990 | 400 |
| **Macro Avg** | **0.986** | **0.986** | **0.986** | **1600** |
| **Overall Accuracy** | **--** | **--** | **0.986** | **1600** |

**Movie S1. GT-QCS solidifies speed on skin and plastic surfaces.**

**Movie S2. Gently and easily remove GT-QCS with warm water.**

**Movie S3. Tensile test of GT-QCS film.**

**Movie S4. Compression test of GT-QCS cylinder.**

**Movie S5. Peeling test of GT-QCS gel between porcine skins.**

**Movie S6. Adhesion performance of the GT-QCS on various substrates.**

**Movie S7. Skin condition when using warm water to remove GT-QCS electrodes after long-term wear.**

**Movie S8. Demonstration of multi-person hand gesture recognition**